LETTERS

A tunable synthetic mammalian oscillator

Marcel Tigges[1], Tatiana T. Marquez-Lago[1,2,3], Jörg Stelling[1,2,3] & Martin Fussenegger[1]

Autonomous and self-sustained oscillator circuits mediating the periodic induction of specific target genes are minimal genetic time-keeping devices found in the central and peripheral circadian clocks[1,2]. They have attracted significant attention because of their intriguing dynamics and their importance in controlling critical repair[3], metabolic[4] and signalling pathways[5]. The precise molecular mechanism and expression dynamics of this mammalian circadian clock are still not fully understood. Here we describe a synthetic mammalian oscillator based on an auto-regulated sense–antisense transcription control circuit encoding a positive and a time-delayed negative feedback loop, enabling autonomous, self-sustained and tunable oscillatory gene expression. After detailed systems design with experimental analyses and mathematical modelling, we monitored oscillating concentrations of green fluorescent protein with tunable frequency and amplitude by time-lapse microscopy in real time in individual Chinese hamster ovary cells. The synthetic mammalian clock may provide an insight into the dynamics of natural periodic processes and foster advances in the design of prosthetic networks in future gene and cell therapies.

Synthetic gene circuits that emulate the expression dynamics of living systems provide new insights into the connectivity of genes and proteins in the postgenomic era[6] and they advance our understanding of complex control networks. Circadian pacemakers[7,8] are of particular interest because they coordinate many periodic physiological activities. The mammalian circadian clock consists of a central pacemaker in the suprachiasmatic nuclei of mammalian brains[9], with subsidiary oscillators in most peripheral cell types[4,5,10]. In contrast to neurons in the suprachiasmatic nuclei, peripheral oscillators damp rapidly when disconnected from remote control by the suprachiasmatic nuclei[10]. However, both oscillators rely on a very similar gene circuitry that involves a set of transcriptional repressors (CRY and PER) and activators (BMAL1 and CLOCK) connected by mutual feedback[11]. Previously designed simple synthetic gene networks in bacteria showed self-sustained[12], damped[13] or metabolically controlled oscillations[14], but those oscillators lacked robustness and/or tunability. In mammalian cells, even synthetic clock replicas using natural components and network design have not provided oscillating transgene expression[15] as observed for reporter genes plugged

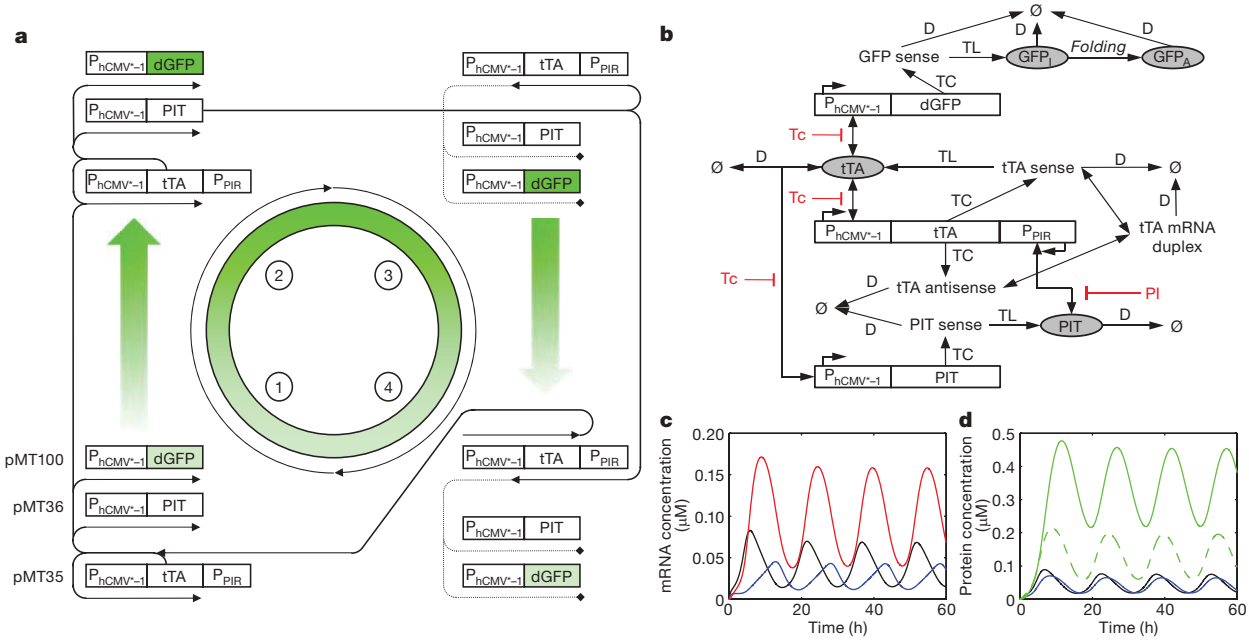

Figure 1 | Mammalian clock components and predicted oscillation dynamics. a, Core mammalian oscillator. Autoregulated $P_{hCMV*-1}$-driven tTA transcription triggers increasing expression of sense tTA (pMT35), Ub^{V76}–GFP (pMT100) and PIT (pMT36) (1). As Ub^{V76}–GFP and PIT levels reach a peak (2), PIT steadily induces P_{PIR}-driven tTA anti-sense expression (3), resulting in a gradual decrease in sense tTA, PIT and Ub^{V76}–GFP (4). **b**, Intracellular processes considered in the mathematical model. Abbreviations and symbols are as follows: single-headed arrows, irreversible reactions; double-headed arrows, reversible reactions; Ø, sinks for degradation processes; dGFP, destabilized GFP; Tc, tetracycline; PI, pristinamycin I; GFP_I, unfolded inactive GFP; GFP_A, folded active GFP; TC, transcription; TL, translation; D, degradation. **c**, **d**, Model predictions for the reference parameter set (plasmid ratios 1:1:1, no antibiotics) with mRNA concentrations (**c**) (black, tTA; blue, PIT; red, tTA-sense–antisense duplex) and protein concentrations (**d**) (black, tTA; blue, PIT; dashed green, unfolded GFP; solid green, active GFP).

[1]Department of Biosystems Science and Engineering, ETH Zurich, Mattenstrasse 26, CH-4058 Basel, Switzerland. [2]Institute of Computational Science and [3]Swiss Institute of Bioinformatics, ETH Zurich, CH-8092 Zurich, Switzerland.

into the natural circadian clock of peripheral fibroblasts[10]. This suggested that important details on how cellular clocks operate are still unknown.

Our synthetic core oscillator (Fig. 1a) consists of a sense–antisense expression unit encoding the tetracycline-dependent transactivator (tTA)[16]. tTA manages its sense transcription by means of an autoregulated feedback loop controlled by the tTA-specific tetracycline-responsive promoter ($P_{hCMV*-1}$; $P_{hCMV*-1}$→tTA; pMT35). Antisense transcription of tTA is driven by the pristinamycin-responsive promoter (P_{PIR}; $P_{hCMV*-1}$→tTA←P_{PIR}; pMT35) and triggered by the pristinamycin-dependent transactivator (PIT)[17], whose expression is induced by $P_{hCMV*-1}$ and thus feedback controlled by tTA ($P_{hCMV*-1}$→PIT; pMT36). tTA levels can be examined by tTA-specific $P_{hCMV*-1}$-driven expression of a fluorescent protein. For reasons given below, we used either the destabilized enhanced yellow fluorescent protein (d2EYFP; $P_{hCMV*-1}$→d2EYFP; pBP282 (ref. 18); see Supplementary Information) or the green fluorescent protein (GFP) variant Ub^{V76}–GFP ($P_{hCMV*-1}$→Ub^{V76}–GFP; pMT100), which have different half-lives. The network can be fine-tuned by modulating sense expression of tTA and PIT by tetracycline and by adjusting tTA antisense transcription by pristinamycin I (PI). In the absence of antibiotics $P_{hCMV*-1}$ and P_{PIR} are fully induced.

To analyse whether the circuit could function as a genetic oscillator, we developed a first deterministic mathematical model (see Supplementary Information). It describes in a simplified yet mechanistic fashion the processes shown in Fig. 1b. Biologically plausible model parameterization demonstrated the oscillatory capacity of the mammalian circuit (Fig. 1c, d). It can undergo autonomous and self-sustained oscillation of tTA expression by alternating the induction of tTA by means of its autoregulated feedback (tTA induces its own expression), with time-delayed repression of tTA mediated by the two-level tTA antisense transcription cascade (tTA triggers PIT expression; PIT then induces tTA antisense expression). The antisense-mediated decrease in tTA levels triggers the recovery of tTA sense expression and, hence, a second clock cycle.

A first oscillator implementation with the d2EYFP reporter provided evidence that the basic design could function *in vivo* (see Supplementary Information). For detailed circuit design, we adapted the model parameters to the experimental d2EYFP time courses from oscillating cells and controls. The refined model enabled us to make a semiquantitative description of the circuit behaviour by capturing all qualitative dynamic features, but not all quantitative aspects (Supplementary Fig. 1 and Supplementary Information). With the experimentally constrained model, we conducted simulation studies with varying model parameters and/or inputs to establish critical design features. The model predicted that the circuit should be robust to variations in protein and messenger RNA degradation and that the antibiotics may switch the oscillator on or off but not tune its behaviour gradually (Supplementary Fig. 2 and Supplementary Notes). Moreover, model analysis suggested that the synthetic network could sustain autonomous oscillations only at specific relative levels of the individual clock components (Fig. 2a, b). These levels are influenced by the relative amounts of expression vectors used to transfect mammalian cells[19]. The model predicted that, even when the ratios of oscillator components were held constant, absolute plasmid concentrations could be used to modify the period and amplitude of the oscillations (Fig. 2a, b). More intuitively, destabilization of the reporter was predicted to increase the relative signal amplitude (Fig. 2b, c). The model-based analysis therefore pointed to reporter stability and gene dosage as key variables for optimizing the circuit.

To reveal any rhythmic transcription control in single cell-based time-lapse microscopy studies, we implemented a second-generation oscillator by functionally plugging in a $P_{hCMV*-1}$-driven GFP variant engineered for a decreased half-life of a few minutes (Ub^{V76}–GFP; pMT100, $P_{hCMV*-1}$→Ub^{V76}–GFP). Co-transfection of pMT35 ($P_{hCMV*-1}$→tTA←P_{PIR}) and pMT100 resulted in a steady increase in green fluorescence, indicating that sense tTA was co-inducing its own expression as well as that of Ub^{V76}–GFP (Supplementary Fig. 3a). We observed a similar increase in Ub^{V76}–GFP expression after co-transfection of pMT100, pMT35 and pMT36 ($P_{hCMV*-1}$→PIT) when transfected populations were cultivated in the presence of PI, which inactivated PIT and prevented tTA antisense expression (Supplementary Fig. 3b). When the same population was exposed to tetracycline, Ub^{V76}–GFP expression was gradually shut off as a result of tTA inactivation (Supplementary Fig. 3c). Ub^{V76}–GFP expression was also shut off when co-transfecting pMT100 and pMT35 with the constitutive PIT expression vector pMF156 (P_{hCMV}→PIT)[17], which confirmed that PIT-mediated induction of P_{PIR}-driven tTA antisense expression outcompetes autoregulated tTA expression (Supplementary Fig. 3d). The individual feedback loops therefore operated as expected.

To test the complete synthetic oscillator we co-transfected pMT35, pMT36 and pMT100 at various ratios. Ratios of 2:1:1 or 3:1:1 resulted in imbalanced expression of clock components and constant expression of Ub^{V76}–GFP (Supplementary Fig. 3e, f). When pMT35, pMT36 and pMT100 were co-transfected at equimolar ratios (100 ng each) into Chinese hamster ovary (CHO-K1) cells cultivated without antibiotics, we observed spontaneous, autonomous, self-sustained and robust oscillations of Ub^{V76}–GFP fluorescence in single cells (Fig. 3 and Supplementary Video). The oscillations could only be disturbed deliberately by adding either tetracycline or PI (Supplementary Fig. 3b, c), or by constitutive PIT expression (Supplementary Fig. 3d). Fast Fourier transformation-based analysis (see Supplementary Information) of at least 20 CHO-K1 cells with oscillating Ub^{V76}–GFP expression collected from four independent experiments showed that oscillations occur at a frequency of 170 ± 71 min (mean ± s.d.), with an amplitude of 1.81 ± 1.96 fluorescence units (Fig. 3). The oscillations of the synthetic clock showed substantial variability between individual cells, even adjacent ones, suggesting that there is no functional coupling between oscillating cells.

Next, to check the model predictions on gene-dosage-dependent oscillator behaviour, we varied the DNA doses used for transfection. In comparison with the oscillations generated by co-transfection of 100 ng pMT35, pMT36 and pMT100 (Fig. 3), co-transfection of 200 ng of each clock vector resulted in oscillation with a higher frequency (period of 147 ± 58 min) but a reduced amplitude

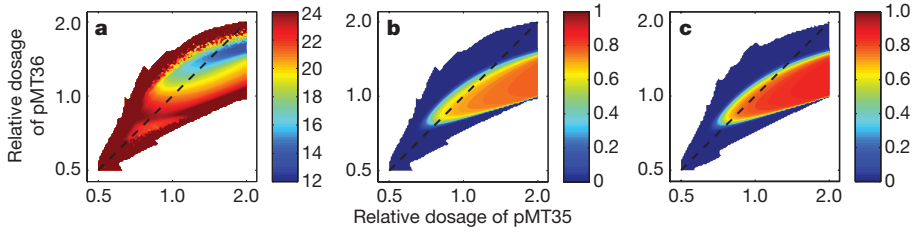

Figure 2 | Systems behaviour depending on gene dosage as predicted by the adapted model with variable transfection times. Panels show the colour-coded oscillator period (**a**; the colour bar gives the period in hours) and relative amplitude (**b**, **c**; normalized by maximal fluorescence) as a function of relative plasmid concentrations. In **a** and **b** the reporters are d2EYFP; in **c** the reporter is Ub^{V76}–GFP, a variant with a decreased half-life. The dashed line denotes a 1:1 plasmid ratio. No oscillations were observed in white areas.

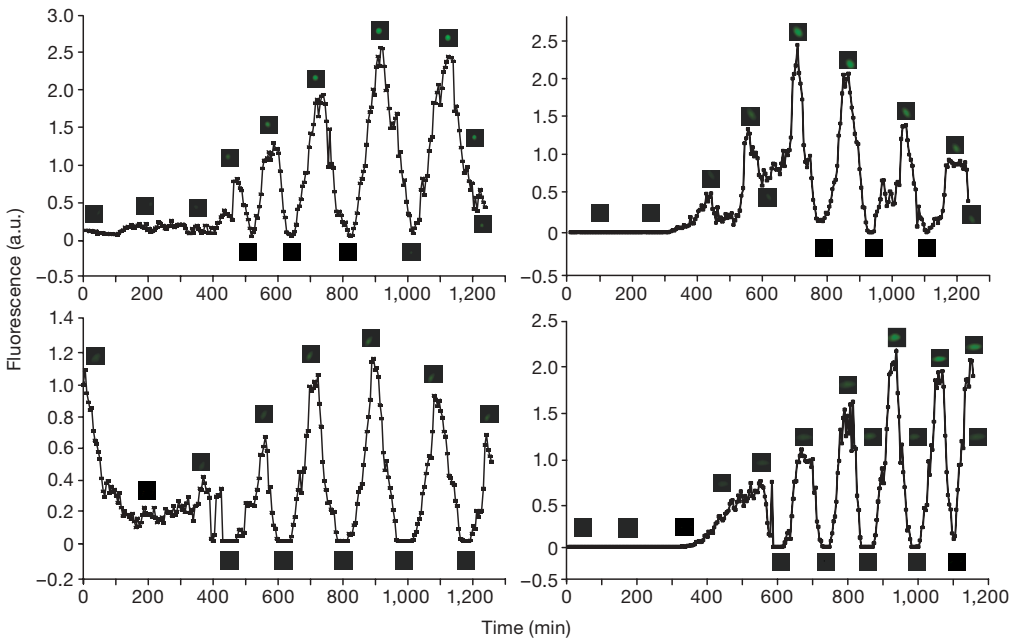

Figure 3 | Validation of the mammalian oscillator by time-lapse fluorescence analysis of transfected CHO-K1 cells. CHO-K1 cells were co-transfected at equimolar ratios (100 ng each) with pMT35 ($P_{hCMV*\text{-}1}$→tTA←P_{PIR}), pMT36 ($P_{hCMV*\text{-}1}$→PIT) and pMT100 ($P_{hCMV*\text{-}1}$→Ub^{V76}–GFP) and cultivated in the absence of antibiotics. The same four independent CHO-K1 cells showing oscillating Ub^{V76}–GFP are also shown, circled, in the Supplementary Video.

(1.44 ± 0.74 fluorescence units) (Fig. 4a), as predicted qualitatively by the model (Fig. 2a–c). When the plasmid doses were decreased to 50 ng each, the oscillation period increased (328 ± 162 min) and the amplitude decreased (0.96 ± 0.63 fluorescence units) (Fig. 4b), which confirms the model predictions on the tunability of the synthetic clock. Quantitative statistical analysis of single-cell data for various plasmid dosages revealed the dependences between gene dosage and oscillator frequency and amplitude shown in Fig. 4c, d. We used these experimental data together with the control experiments to establish a structurally refined mathematical model that could describe all experimental data quantitatively (see Supplementary Information). This deterministic model predicted non-intuitive relations between gene dosage and oscillator behaviour (Fig. 4c, d). Thus, our model-supported synthetic biology approach revealed a previously unknown correlation between oscillation frequency and gene dosage of clock components.

Variable timings of plasmid uptake constitute a major source of cell-to-cell variability of GFP expression. However, through the alignment of single-cell trajectories by using simplified models (see Supplementary Information), we estimated that GFP expression in control experiments varied by only about 20%. Previous studies pointed to stochasticity, or 'noise', as a principal reason for limiting accuracy in synthetic networks[20,21]. To estimate the impact of molecular noise on the mammalian oscillator, we established a detailed stochastic model (see Supplementary Information). Stochastic simulations show that, at least for low plasmid dosages, noise contributes substantially to the observed cell-to-cell variability in the period (Fig. 4c, d). The model predicts that not all cells will

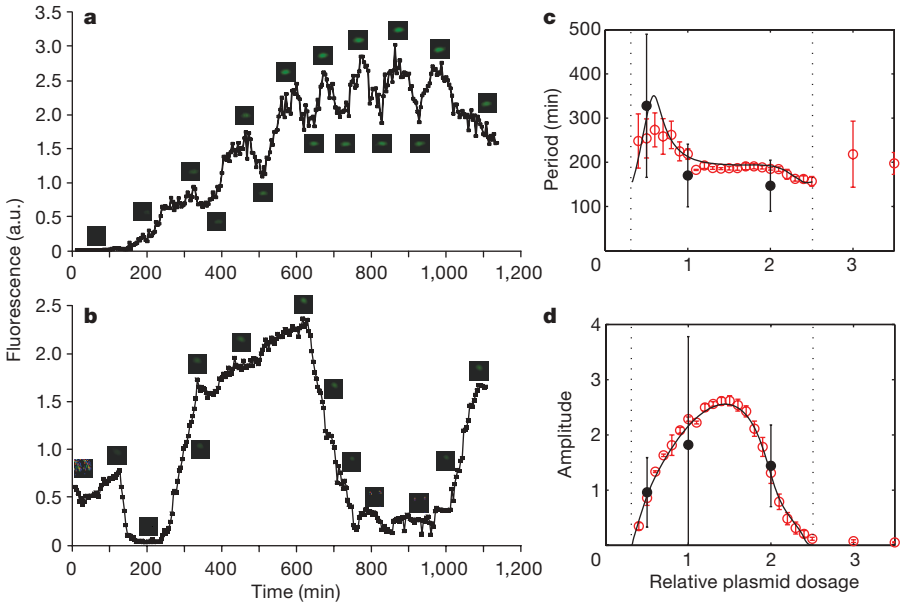

Figure 4 | Tunable oscillating gene expression in mammalian cells. Examples of oscillating CHO-K1 cells co-transfected at equimolar ratios (**a**, 200 ng each; **b**, 50 ng each) with pMT35, pMT36 and pMT100 in cultivation without antibiotics. **c**, **d**, Statistical data analysis and model predictions for oscillator period (**c**) and amplitude (**d**). Experimental data from at least 20 single-cell trajectories per plasmid dosage (filled black symbols; a relative plasmid dosage of one corresponds to 100 ng of DNA) and predictions from the refined deterministic model (black lines) and from stochastic simulations (red symbols) for a similar number of oscillations. Dotted lines indicate regions of oscillations for the deterministic model. Error bars indicate s.d.

oscillate under these conditions. In addition, we find low-amplitude noise-induced oscillations for high plasmid dosages that are similar to those predicted for simplified oscillators[21]. This underlines the importance of stochastic effects on the quantitative behaviour of systems with complicated dynamics[22].

Prokaryotic clocks that were constructed previously[12–14] employed only transcription control elements, and it was not obvious whether a post-transcriptional control component in a mammalian circuit could enable autonomous and self-sustained oscillations. The recent discovery of antisense clock-gene transcripts suggests that mechanisms of gene regulation operating through antisense RNA may also be integral to the circadian clockwork and be more important than previously anticipated[23]. Using a novel network design combining an autoregulated positive transcription feedback with a two-step transcription cascade producing non-coding antisense RNA for translation control, we achieved autonomous, self-sustained and tunable oscillation in mammalian cells. Besides providing insight into the dynamics of mammalian clocks, a more profound understanding of molecular time-keeping devices could foster therapeutic opportunities in clock-related pathologies such as Huntington's[24] and Alzheimer's[25] diseases.

METHODS SUMMARY

Design of expression vectors. pcDNA3.1-Ub^{V76}–GFP enables the constitutive expression of the destabilized GFP variant Ub^{V76}–GFP[26]. pMT35 ($P_{hCMV*\text{-}1}$→tTA←P_{PIR}) contains an expression unit for the $P_{hCMV*\text{-}1}$-driven sense and P_{PIR}-driven antisense expression of tTA[17,27]. pMT35 was constructed by replacing $p27^{Kip1}$ of pMF226 (ref. 27) with tTA of pSAM200 by using EcoRI/HindIII. pMT36 ($P_{hCMV*\text{-}1}$-PIT), engineered for $P_{hCMV*\text{-}1}$-driven PIT[17] expression, was constructed by elimination of the NotI fragment from pMF125 (ref. 28). pMT100 ($P_{hCMV*\text{-}1}$-Ub^{V76}–GFP), enabling the tetracycline-responsive expression of Ub^{V76}–GFP, was designed by inserting Ub^{V76}–GFP, excised from pcDNA3.1-Ub^{V76}–GFP by NheI/NotI, into the corresponding sites of pMF111 (ref. 29). pMF156 encodes the constitutive expression of PIT (P_{hCMV}→PIT)[17].

Cell culture, transfection and gene regulation. CHO-K1 (ATCC CCL61) cells were cultivated in ChoMaster HTS (Cell Culture Technologies) supplemented with 5% fetal calf serum (lot no. P231902; Pan Biotech GmbH). Cells were cultivated at 30 °C in a humidified atmosphere containing 5% CO_2, and 35,000 cells were transfected with up to 1.2 μg of plasmid mixtures by using the FuGENE6 transfection reagent (lot no. 93535720; Roche Molecular Biochemicals).

Fluorescence imaging. Time-lapse fluorescence microscopy was performed with an inverted fluorescent microscope (DMI 6000B; Leica Microsystems) equipped with an incubation chamber, a DFC350FX R2 digital camera (Leica), a 10× objective (Obj. HC PL FL 10×/0.30 PH1 –/D 11.0; Leica) and a 488-nm/509-nm (B/G/R) Ub^{V76}–GFP-specific excitation/emission filter set. Time-lapse videos were produced with the LAS AF imaging software (FW4000-TZ; Leica) set to exposure times of 590–960 ms (auto-controlled depending to the mean fluorescence intensity level) every 3 min. Fluorescence was quantified with ImageJ software for at least 50 cells per condition.

Computational modelling. All details of mathematical models and computational methods are provided in Supplementary Information. Simulations were performed with MATLAB (MathWorks).

Received 26 July; accepted 4 November 2008.

1. Gillette, M. U. & Sejnowski, T. J. Physiology. Biological clocks coordinately keep life on time. *Science* **309,** 1196–1198 (2005).
2. Schibler, U. & Sassone-Corsi, P. A web of circadian pacemakers. *Cell* **111,** 919–922 (2002).
3. Lahav, G. The strength of indecisiveness: oscillatory behavior for better cell fate determination. *Sci. STKE* **2004,** pe55 (2004).
4. Kaasik, K. & Lee, C. C. Reciprocal regulation of haem biosynthesis and the circadian clock in mammals. *Nature* **430,** 467–471 (2004).
5. Covert, M. W., Leung, T. H., Gaston, J. E. & Baltimore, D. Achieving stability of lipopolysaccharide-induced NF-κB activation. *Science* **309,** 1854–1857 (2005).
6. Hasty, J., McMillen, D. & Collins, J. J. Engineered gene circuits. *Nature* **420,** 224–230 (2002).
7. Reppert, S. M. & Weaver, D. R. Forward genetic approach strikes gold: cloning of a mammalian clock gene. *Cell* **89,** 487–490 (1997).
8. Storch, K. F. *et al.* Extensive and divergent circadian gene expression in liver and heart. *Nature* **417,** 78–83 (2002).
9. Reppert, S. M. & Weaver, D. R. Coordination of circadian timing in mammals. *Nature* **418,** 935–941 (2002).
10. Nagoshi, E. *et al.* Circadian gene expression in individual fibroblasts: cell-autonomous and self-sustained oscillators pass time to daughter cells. *Cell* **119,** 693–705 (2004).
11. Gekakis, N. *et al.* Role of the CLOCK protein in the mammalian circadian mechanism. *Science* **280,** 1564–1569 (1998).
12. Atkinson, M. R., Savageau, M. A., Myers, J. T. & Ninfa, A. J. Development of genetic circuitry exhibiting toggle switch or oscillatory behavior in *Escherichia coli*. *Cell* **113,** 597–607 (2003).
13. Elowitz, M. B. & Leibler, S. A synthetic oscillatory network of transcriptional regulators. *Nature* **403,** 335–338 (2000).
14. Fung, E. *et al.* A synthetic gene–metabolic oscillator. *Nature* **435,** 118–122 (2005).
15. Chilov, D. & Fussenegger, M. Toward construction of a self-sustained clock-like expression system based on the mammalian circadian clock. *Biotechnol. Bioeng.* **87,** 234–242 (2004).
16. Gossen, M. & Bujard, H. Tight control of gene expression in mammalian cells by tetracycline-responsive promoters. *Proc. Natl Acad. Sci. USA* **89,** 5547–5551 (1992).
17. Fussenegger, M. *et al.* Streptogramin-based gene regulation systems for mammalian cells. *Nature Biotechnol.* **18,** 1203–1208 (2000).
18. Kramer, B. P. & Fussenegger, M. Transgene control engineering in mammalian cells. *Methods Mol. Biol.* **308,** 123–143 (2005).
19. Rossmanith, W., Chabicovsky, M., Herkner, K. & Schulte-Hermann, R. Cellular gene dose and kinetics of gene expression in mouse livers transfected by high-volume tail-vein injection of naked DNA. *DNA Cell Biol.* **21,** 847–853 (2002).
20. Rosenfeld, N., Young, J. W., Alon, U., Swain, P. S. & Elowitz, M. B. Gene regulation at the single-cell level. *Science* **307,** 1962–1965 (2005).
21. Vilar, J. M., Kueh, H. Y., Barkai, N. & Leibler, S. Mechanisms of noise-resistance in genetic oscillators. *Proc. Natl Acad. Sci. USA* **99,** 5988–5992 (2002).
22. Di Ventura, B., Lemerle, C., Michalodimitrakis, K. & Serrano, L. From *in vivo* to *in silico* biology and back. *Nature* **443,** 527–533 (2006).
23. Crosthwaite, S. K. Circadian clocks and natural antisense RNA. *FEBS Lett.* **567,** 49–54 (2004).
24. Morton, A. J. *et al.* Disintegration of the sleep–wake cycle and circadian timing in Huntingdon's disease. *J. Neurosci.* **25,** 157–163 (2005).
25. Wu, Y. H. *et al.* Pineal clock gene oscillation is disturbed in Alzheimer's disease, due to functional disconnection from the 'master clock'. *FASEB J.* **20,** 1874–1876 (2006).
26. Johnson, E. S., Ma, P. C., Ota, I. M. & Varshavsky, A. A proteolytic pathway that recognizes ubiquitin as a degradation signal. *J. Biol. Chem.* **270,** 17442–17456 (1995).
27. Fux, C. *et al.* Streptogramin- and tetracycline-responsive dual regulated expression of $p27^{Kip1}$ sense and antisense enables positive and negative growth control of Chinese hamster ovary cells. *Nucleic Acids Res.* **29,** e19 (2001).
28. Moser, S. *et al.* Dual-regulated expression technology: a new era in the adjustment of heterologous gene expression in mammalian cells. *J. Gene Med.* **3,** 529–549 (2001).
29. Fussenegger, M., Schlatter, S., Datwyler, D., Mazur, X. & Bailey, J. E. Controlled proliferation by multigene metabolic engineering enhances the productivity of Chinese hamster ovary cells. *Nature Biotechnol.* **16,** 468–472 (1998).

Supplementary Information is linked to the online version of the paper at www.nature.com/nature.

Acknowledgements We thank H. Meyer for providing pcDNA3.1-Ub^{V76}–GFP; and B. Kramer, M. Gitzinger, D. Greber and W. Weber for conceptual input and/or critical comments on the manuscript. This work was supported by the Swiss National Science Foundation and the EC Framework 6 (COBIOS).

Author Information Reprints and permissions information is available at www.nature.com/reprints. Correspondence and requests for materials should be addressed to M.F. (fussenegger@bsse.ethz.ch) or J.S. (joerg.stelling@bsse.ethz.ch).